$Ta_{11}Si_2Se_8$ – Condensed Tetrakaidecahedral Ta_9Si Clusters Arranged to an Open Network Structure

Antje Mrotzek and Bernd Harbrecht*[a]

Dedicated to Professor Edgar Niecke on the occasion of his 60th birthday

Keywords: Selenium / Silicon / Silicides / Tantalum / Condensed cluster compounds

$Ta_{11}Si_2Se_8$ was synthesized from a pre-reacted mixture of the elements in a sealed tantalum tube at 1570 K. Mo-doped crystals were obtained in a welded molybdenum crucible by a chemical transport reaction using TeI_4 as a transport agent. The structure of $Mo_{0.11}Ta_{10.89(2)}Si_2Se_8$ has been determined by single crystal X-ray means [*Pnnm*, $Z = 2$, $a = 1184.4(1)$ pm, $b = 1939.4(1)$ pm, $c = 346.48(2)$ pm, $wR_2 = 0.069$]. The structure of the ternary phase was verified by means of a Rietveld profile fit of a powder X-ray diffractogram. The silicide is isotypic with $Ta_{11}Ni_2Se_8$. The structure is composed of Si-centred, tricapped trigonal prismatic Ta_9Si clusters. The tetrakaidecahedral Ta_9Si clusters are fused into twin chains by sharing the Ta^{pr} atoms of facing triangulated prism faces and one out of three capping atoms Ta^c. Intercluster linkage of the remaining Ta^c atoms generates a microporous $^3_\infty[SiTa_2^c\ Ta_{1/2}^c\ Ta_{6/2}^{pr}]$ substructure. The channels of the metal network are sheathed by three-, four-, five-, and sixfold coordinated Se atoms. Four-probe dc resistivity measurements revealed the Mo-doped phase to be a moderate metallic conductor. The bonding interactions contributing to the stability of $Ta_{11}Si_2Se_8$ and distinctions in bonding for $Ta_{11}Si_2Se_8$ and $Ta_{11}Ni_2Se_8$ are analysed on the basis of semi-empirical extended Hückel calculations.

Introduction

Tantalum is known to form numerous metal-rich chalcogenides with very distinctive and partly exotic structural and/or physical properties. By using the versatile metal partial structure as a guideline, four groups of tantalum subchalcogenides can be distinguished:

(1) Interpenetrating metal-centred icosahedral structures: Much of the motivation for exploring low-valent tantalum chalcogenides goes back to the findings of Franzen and Smeggil[1] that tantalum can form frameworks based on interpenetrating metal-centred icosahedra. The structures of the sulfides Ta_6S_n ($n = 1$,[1][2] 3,[1] and 4[3]), $M_xTa_{6-x}S$ (M = V, Cr),[4] $AuTa_5S$,[5] $M_xTa_{15-x}S_2$ (M = Au, Al, Ga, Ge, Sn, Sb, Pd, Pt, Rh, Ir)[6] are examples of such clusters. The small-band-gap semiconductor Ta_6Te_5[7] with a unique one-dimensional pentagonal antiprismatic chain structure, the layer-type chalcogenides $Ta_3(S,Se)_2$,[8] $Ta_5(Se,Te)_3$,[9] and $Ta_3(S,Te)_2$,[10] as well as $Ta_5(S,Te)_2$[11] exhibiting a perforated Ta partial structure and the unprecedented quasicrystalline chalcogenide $Ta_{2\sqrt{3}+3}Te_4$,[7b][12] marked by a Fourier spectrum with twelvefold rotational symmetry, belong to this group of structures. They all are composed of interpenetrating, condensed, or metal−metal-bonded M_{13} icosahedra and/or fragments thereof.

(2) Body-centred cubic fragment-structures: The structures of several other low-valent tantalum chalcogenides have in common that parts of the body-centred cubic (*bcc*) arrangement of tantalum are preserved. In contrast to sulphur, tellurium, vanadium, and chromium, homologous elements like selenium, niobium, molybdenum, and tungsten promote the formation of *bcc* fragment structures. Representatives of this group are the metal-rich layer-type structures Ta_2Se, $Ta_2(S,Se)$ [$n(S)/n(Se) < 4$], $Ta_5(S,Se)_2$, $Ta_9(S,Se)_4$, $M_xTa_{5-x}S_2$ (M = Mo, W), $(Nb,Ta)_2S$, and $(Nb,Ta)_5S_2$[13] and the network structures of $(Nb,Ta)_{11}S_4$ and $(Nb,Ta)_9(S,Te)_5$.[14]

(3) Quasi-one-dimensional metal-rich chalcogenides: The structures of some rare examples of this third group consist of columnar metal cores completely covered with chalcogen atoms; van der Waals interactions provide the cohesion of the strings. The tellurides M_4ETe_4 (M = Nb, Ta; E = Si, Cr, Fe, Co, Ni),[15] e.g., are composed of chains of confacial square antiprismatic clusters, $^1_\infty[SiTa_{8/2}Te_{8/2}]$. Deintercalated $LiMo_3Q_3$ (Q = Se, Te)[16] and Ta_6Te_5[7] show similar structural features.

(4) Condesed tetrakaidecahedral cluster compounds: The compounds of the fourth group contain, in addition to sulphur or selenium, an iron-group metal as a second minor component. As a consequence of a substantial difference between the Ta−Q and M−Q affinities, the partial structures of the 3d-metal and chalcogen components are spatially separated by the intermediate partial structure of the major component. At low contents of the 3d metal, the M atoms are encapsulated in tricapped trigonal prismatic Ta_9 clusters confined by 14 triangular faces. All structures of this type known so far contain columns of condensed tetrakaidecahedral clusters. The columns, however, can be linked in different ways giving rise to a variety of compositionally distinct compounds: $Ta_9M_2S_6$, $Ta_{11}M_2Se_8$ (M = Fe, Co, Ni)

[a] Fachbereich Chemie, Philipps-Universität Marburg,
Hans-Meerwein-Straße 1, D-35032 Marburg, Germany
Fax: (internat.) + 49(0)6421/288917
E-mail: fkc@mail.chemie.uni-marburg.de

  1434−1948/99/0101−0087 $ 17.50+.50/0

and Ta_8MSe_8 (M = Co, Ni),[17] $M_{1-x}Nb_6S_{2+x}$ (M = Fe, Co, Ni, Cu), $M_{2-x}Nb_9S_{3+x}$ and $M_{2-x}Nb_8S_{4+x}$ (M = Co, Ni),[18] Hf_8MTe_6 (M = Mn, Fe), Hf_5MTe_3 (M = Fe, Co), and Zr_6MTe_2 (M = Mn, Fe, Co, Ni, Ru, Pt).[19]

In an attempt to expand the structural chemistry of tantalum-rich chalcogenides by including another main-group element we explored selected ternary tantalum-selenium systems containing a group-14 element as a minor component.[20] Here we report the synthesis and structure of a tantalum-rich silicide selenide $Ta_{11}Si_2Se_8$ which is isotypic with the compounds of the $Ta_{11}M_2Se_8$ (M = Fe, Co, Ni)[17c,d] series.

Results and Discussion

Synthesis, Analyses, Electrical Properties

Microcrystalline, single-phase $Ta_{11}Si_2Se_8$ was obtained by a gas-solid reaction from a pre-reacted stoichiometric mixture of the elements in welded tantalum tubes at 1570 K within 2 days. The results of a Rietveld refinement are shown in Figure 1. Data on the profile fit are given in Table 1. Fibrous crystals up to 3 mm in length and 20 μm in diameter (Figure 2) were obtained by a chemical vapour transport reaction in welded molybdenum crucibles using TeI_4 as a transport agent. Energy-dispersive X-ray spectroscopy (EDX) and X-ray single crystal structure analyses revealed the presence of some molybdenum in the samples. No indication of an enrichment of tellurium was obtained. The results of a structure refinement of $Mo_{0.11}Ta_{10.89(2)}Si_2Se_8$ are listed in Tables 2, 3, and 4. As expected for a metal-rich compound with extended metal−metal bonding, $Ta_{11}Si_2Se_8$ is a moderate metallic conductor. The resistivity increases steadily with increasing temperature. The values for two different samples were found to be about 1 mΩcm and 1.5 mΩcm at 10 K and 1.6 mΩcm and 2.1 mΩcm at 320 K, respectively.

Table 1. Selected parameters of the Rietveld analysis of $Ta_{11}Si_2Se_8$

Measuring parameters		
Scan-range, stepwidth (2θ) [°]		5.00−95.00 / 0.03
Total measuring time [h]		50
Radiation		Cu-K_α
Global parameters		
Number of phases		1
Number of variables		45
Profile fit		pseudo-Voigt
Background		refined
Structure and profile data		
Formula mass [g mol^{-1}]		2678.28
Space group (No.)		*Pnnm* (58)
Lattice parameters: *a* [pm]		1181.44(4)
b [pm]		1937.24(6)
c [pm]		346.33(1)
V [10^{6}pm^3]		792.66(7)
Formula units per cell		2
Coefficients for peak FWHM	*U*	0.095(7)
	V	−0.063(4)
	W	0.022787)
Preferred orientation		[0 0 1]
Perferred orientation parameter		1.189(4)
Asymmetry parameter		0.32(2)
Peak shape parameter η		0.83(2)
R_P		0.0457
R_{WP}		0.0643
R_B		0.0182

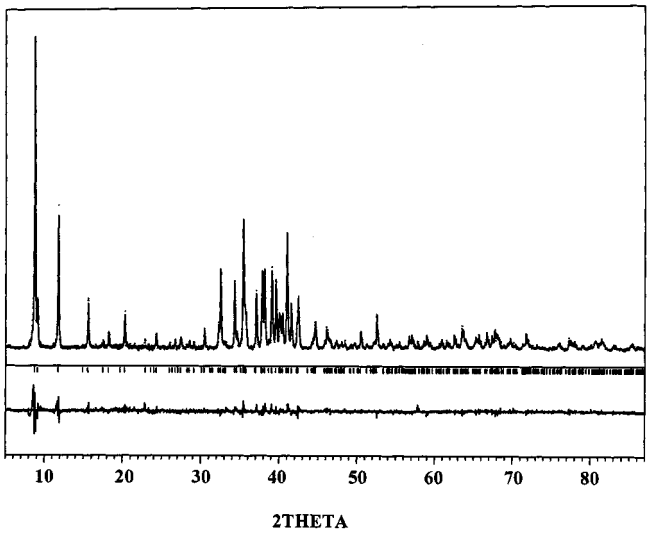

Figure 1. Rietveld profile fit of a powder X-ray diffractogram (Cu-K_α) of $Ta_{11}Si_2Se_8$, measured (points) and calculated (line) diffractogram (top), Bragg positions (middle), and difference plot (bottom)

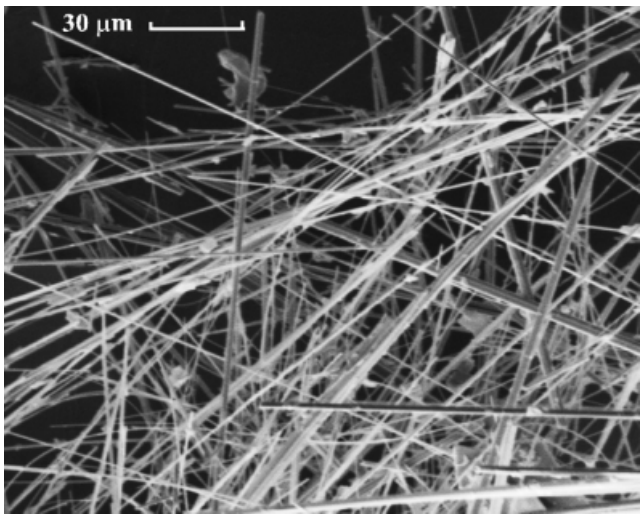

Figure 2. Scanning electron micrograph of needle-shaped crystals of $Mo_xTa_{11-x}Si_2Se_8$ transported to the lid of the molybdenum crucible

Description of the Crystal Structure

The structure is composed of eleven crystallographically inequivalent atoms: Ta1−Ta6, Si1, and Se1−Se4. They all are located in mirror planes perpendicular to the short *c* axis at *z* = 0 and 1/2 modulo 1. Figure 3 shows the structure in a projection along the short *c* axis. The basic unit of the structure is an Si-centred tricapped trigonal prism, i.e. a tetrakaidecahedral Ta_9Si cluster that is confined by fourteen triangular faces. Strong interactions between the

Table 2. Data collection and refinement parameters of $Mo_{0.11}Ta_{10.89(2)}Si_2Se_8$[a]

Crystal data	
Chemical formula	$Mo_{0.11}Ta_{10.89(2)}Si_2Se_8$
Formula mass [g mol^{-1}]	2668.37
Space group (No.)	*Pnnm* (58)
a [pm]	1184.4(1)
b [pm]	1939.4(1)
c [pm]	346.48(2)
V [10^6 pm^3]	795.9(1)
Z	2
ρ_X [g cm^{-3}]	11.137
μ [cm^{-1}]	92.99
Data collection	
Crystal size [mm]	0.02 × 0.02 × 0.31
Diffractometer	IPDS
Radiation	Mo-K_α
Monochromator	Graphite
Detector distance [mm]	50
Rotation range ϕ [°], $\phi_{incr.}$ [°]	0–200, 1
Bragg angle $2\theta_{max}$ [°]	60.9
Reflections measured	$h \leq \pm 16$, $k \leq \pm 27$, $l \leq \pm 4$
Number of reflections	9296
Completeness of data set	99.3%
Data reduction	
Program	XPREP[25b]
Absorption correction	semi-empirical
min./max. transmission	0.360/0.483
Number of unique reflections	1353
R_{int} (*F*)	0.0761
Refinement	
Program	SHELXL-96[25c]
Number of parameters	66
Number of reflections $F_o > 4\sigma(F_o)$	997
R_1 [$F_o > 4\sigma(F_o)$]/R_1 (all)	0.0289 / 0.0427
wR_2	0.0691
Goof	0.902
$\Delta\rho_{max}/\Delta\rho_{min}$ [10^{-6} e pm^{-3}]	4.06/–3.56

[a] Further details of the crystal structure determination may be obtained from the Fachinformationszentrum Karlsruhe, D-76344 Eggenstein-Leopoldshafen (Germany), on quoting the depository number CDS-408960.

Table 3. Positional parameters and displacement parameters U_{eq} [pm^2] of $Mo_{0.11}Ta_{10.89(2)}Si_2Se_8$; $z = 0$

	Wyckoff	*x*	*y*	U_{eq}
Ta1/Mo1[a]	*2a*	0	0	23(4)
Ta2	*4g*	0.33926(5)	0.28621(3)	24(1)
Ta3	*4g*	0.32286(5)	0.85596(3)	21(1)
Ta4	*4g*	0.43448(5)	0.61311(3)	23(1)
Ta5	*4g*	0.04949(5)	0.24242(3)	27(1)
Ta6	*4g*	0.32096(5)	0.45315(3)	23(1)
Se1	*4g*	0.1070(1)	0.44655(9)	40(3)
Se2	*4g*	0.4585(1)	0.17258(9)	35(3)
Se3	*4g*	0.2137(1)	0.05741(9)	32(3)
Se4	*4g*	0.2845(1)	0.71315(9)	24(3)
Si1	*4g*	0.0921(4)	0.8715(2)	22(7)

[a] Occupation factors: $b_{Ta1} = 0.89(2)$, $b_{Mo1} = 0.11$.

central Si and the peripheral Ta^{pr} atoms of the prism are indicated by a mean distance of 255.2 pm. The three capping Ta^c atoms are somewhat more distant (274.8 pm). Ta–Ta bonds contribute significantly to the stability of the cluster: The mean d_{Ta1-Ta} between Ta^{pr} and Ta^c atoms is 289.3 pm in contrast to 338.1 pm between Ta atoms of adjacent prisms. The shortest Si–Si distance corresponds to the parameter *c* (346.48 pm). In contrast to the less metal-rich phase Ta_4SiTe_4[15a,b] (d_{Si-Si} = 235.3, 244.8 pm), there are no homonuclear Si–Si bonds in $Ta_{11}Si_2Se_8$.

The clusters are condensed via common trigonal prism faces into columns, according to $^1_\infty[SiTa_{6/2}{}^{pr}Ta_3{}^c]$. Furthermore, two columns share the Ta1 atom of one out of the three capping positions, $^1_\infty[(SiTa_{6/2}{}^{pr}Ta_2{}^cTa_{1/2}{}^c)_2] = Ta_{11}Si_2$. A part of such a twin column is shown in Figure 4. Adjoining twin columns are shifted relative to each other by *c*/2. Intercluster bonding contacts between Ta3 and Ta5 (318.4 pm) link the columns to an open three-dimensional network. The resulting elongated channels are sheathed by four crystallographically inequivalent Se atoms which cover and bridge the clusters in different ways: Se2 with coordination number CN 4, $<d_{Ta-Se1}>$ = 262.8 pm, and Se4 (CN 6, <269.2 pm>) connect adjacent twin columns, while Se1 (CN 3, <258.2 pm>) and Se3 (CN 5, <270.8 pm>) bridge the clusters which share capping Ta atoms. As one can clearly see from Figure 5, the coordination polyhedra of the Se atoms represent distinct fragments of a Ta_9Se cluster related to the Ta_9Si cage. The one-sided coordination of all Se atoms points to a very characteristic structural functionality of the most electronegative component of the compound: the Se atoms saturate the remaining valences of the open $Ta_{11}Si_2$ network structure by completely covering its internal surfaces.

Features of the Electronic Structure

The electronic band structures of $Ta_{11}Si_2Se_8$ and $Ta_{11}Ni_2Se_8$ were calculated with the extended Hückel method.[21] Parameters were taken from the literature,[22] and are listed in Table 5. The valence-state ionization energies H_{ii} and the coefficients of the Slater-type orbitals, c_1 and c_2, for tantalum are based on charge-iterative calculations.[20] Band structure calculations were carried out using a 30 *k* point mesh lying in the representation domain of the corresponding space group. The total density of states (DOS) and the contributions of each component of the compounds are shown in Figure 6. The total DOS of the silicide can be subdivided into four blocks:

(i) The primarily Se 4s based peak around –22 eV is not shown.

(ii) The levels between –18 and –13.5 eV are dominantly of Ta 5d and Se 4p character. Mixing of these orbitals gives rise to strong heteronuclear Ta–Se interactions.

(iii) Above a deep local minimum in the DOS around –13.5 eV a third range of Si p and Ta d based states extends up to the Fermi level. A smaller portion of these states at low energy reflects strong heteronuclear Ta–Si bonds whereas the upper levels correspond basically to extended Ta–Ta bonds. Obviously, the heteronuclear bonding interactions Ta–Se and Ta–Si are segregated energetically and spatially. There are no significant Si–Se interactions ($d_{Se-Si} \geq$ 382.5 pm) contributing to the stability of this compound.

Table 4. Characteristic interatomic distances [pm] of $Mo_{0.11}Ta_{10.89(2)}Si_2Se_8$

Ta1, Mo	− 2 × Si1	272.0(5)	Ta2	− 2 × Si1	253.0(4)	Ta3	− 2 × Se1	260.4(1)
	− 2 × Se3	276.6(2)		− 1 × Se2	261.8(2)		− 1 × Se2	264.8(2)
	− 4 × Ta6	288.50(5)		− 2 × Se4	267.6(1)		− 1 × Si1	275.0(4)
	− 4 × Ta4	290.09(5)		− 2 × Ta3	291.85(7)		− 1 × Se4	280.7(2)
				− 2 × Ta5	308.38(8)		− 2 × Ta2	291.85(7)
				− 1 × Ta6	324.5(1)		− 2 × Ta6	307.49(7)
				− 1 × Ta4	331.57(9)		− 2 × Ta5	318.36(8)
				− 1 × Ta5	353.55(9)			
Ta4	− 2 × Si1	256.4(4)	Ta5	− 2 × Se2	262.3(1)	Ta6	− 1 × Se1	253.8(2)
	− 1 × Se4	263.0(2)		− 2 × Se4	268.1(1)		− 2 × Si1	256.3(4)
	− 2 × Se3	269.3(1)		− 1 × Si1	277.4(5)		− 2 × Se3	269.4(1)
	− 2 × Ta1, Mo	290.09(5)		− 2 × Ta4	305.40(8)		− 2 × Ta1, Mo	288.50(5)
	− 2 × Ta5	305.40(8)		− 2 × Ta2	308.38(8)		− 2 × Ta3	307.49(7)
	− 1 × Ta6	316.87(9)		− 2 × Ta3	318.36(8)		− 1 × Ta4	316.87(9)
	− 1 × Ta2	331.57(9)		− 1 × Ta2	353.55(9)		− 1 × Ta2	324.5(1)
	− 1 × Ta6	338.1(1)					− 1 × Ta4	338.1(1)
Se1	− 1 × Ta6	253.8(2)	Se2	− 1 × Ta2	261.8(2)	Se3	− 2 × Ta4	269.3(1)
	− 2 × Ta3	260.4(1)		− 2 × Ta5	262.3(1)		− 2 × Ta6	269.4(1)
	− 1 × Se1	327.4(3)		− 1 × Ta3	264.8(2)		− 1 × Ta1, Mo	276.6(2)
				− 2 × Se1	338.1(2)			
Se4	− 1 × Ta4	263.0(2)				Si1	− 2 × Ta2	253.0(4)
	− 2 × Ta2	267.6(1)					− 2 × Ta6	256.3(3)
	− 2 × Ta5	268.1(1)					− 2 × Ta4	256.4(3)
	− 1 × Ta3	280.7(2)					− 1 × Ta1, Mo	272.0(5)
	− 2 × Se2	345.1(2)					− 1 × Ta3	275.0(4)
							− 1 × Ta5	277.4(5)

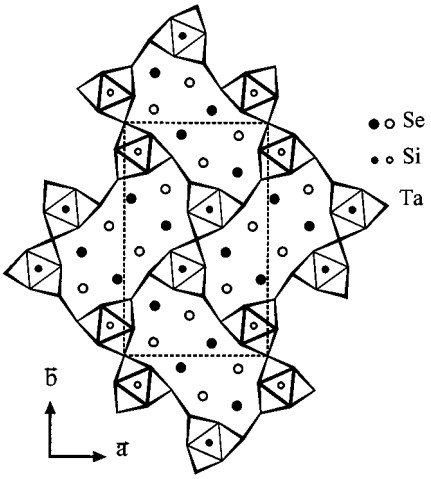

Figure 3. The structure of $Ta_{11}Si_2Se_8$ projected onto the *a,b* plane

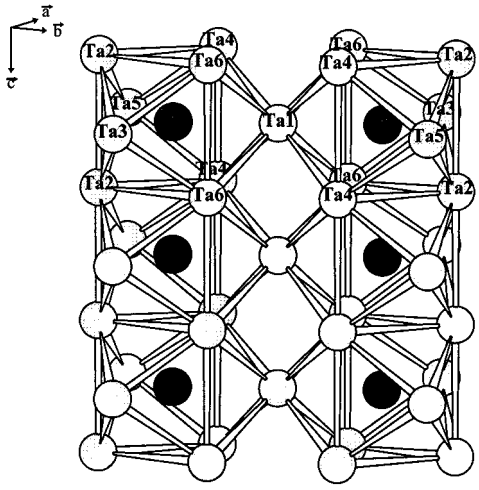

Figure 4. Part of a twin column of condensed Ta_9Si tetrakaidecahedra as present in the structure of $Mo_{0.11}Ta_{10.89(2)}Si_2Se_8$; the columns extend parallel to the short *c* axis

(iv) The states in the 6 eV wide energy window above the Fermi level (−9.8 eV) have mainly Ta d and very little Si p and Se p character. The relatively low electron concentration at the Fermi level may account for the moderate electrical conductivity of $Ta_{11}Si_2Se_8$.

Below the Fermi level the shown DOS of $Ta_{11}Ni_2Se_8$ and $Ta_{11}Si_2Se_8$ can be roughly divided into two blocks separated by a local DOS minimum at about −13.5 eV. Noticeable differences are associated with the position and influence of the states originating from the minor components, Ni and Si. Whereas the states with Ni d character are concentrated in the block at low energy, namely around −14 eV, the states with Si p character are mainly situated somewhat above the local DOS minimum at −13.5 eV in the upper block. Thus, the interactions of the low-lying Se p and Ni d with the Ta d levels give rise to a larger dispersion of the Ta d levels for $Ta_{11}Ni_2Se_8$ than for $Ta_{11}Si_2Se_8$. This difference in the dispersion is also reflected in the position of the Fermi level which resides in a local DOS minimum for the silicide but intersects a local maximum for $Ta_{11}Ni_2Se_8$.

COOP curves (crystal orbital overlap populations) of Ta−Ta, Ta−Se, and Ta−Si are shown in Figure 7. Obviously, the structure of $Ta_{11}Si_2Se_8$ affords an optimal adjustment of homonuclear Ta−Ta and heteronuclear Ta−Si interactions: these bonding states are completely populated; anti-bonding states are empty. Figure 8 illuminates the major structural distinctions of $Ta_{11}Si_2Se_8$ and $Ta_{11}Ni_2Se_8$.

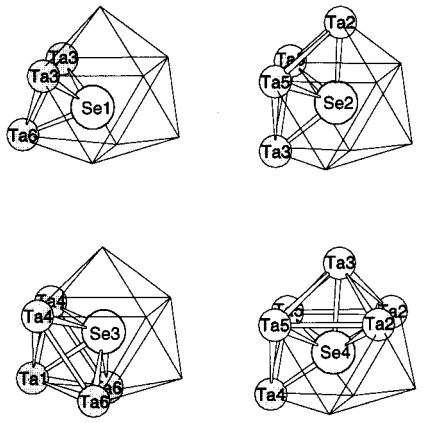

Figure 5. Single-sided Ta coordinations of the four inequivalent Se atoms schematically depicted as fragments of a fictitious Ta_9Se tetrakaidecahedron

Table 5. Parameters for the extended Hückel calculations

Element	Orbital	H_{ii} [eV]	ζ_1	ζ_2	c_1	c_2
Ta	6s	−8.88	2.28	–	–	–
	6p	−5.83	2.24	–	–	–
	5d	−10.39	4.76	1.94	0.6815	0.6815
Se[22a]	4s	−20.50	2.44	–	–	–
	4p	−14.40	2.07	–	–	–
Si[15b]	3s	−17.30	1.38	–	–	–
	3p	−9.20	1.38	–	–	–
Ni[22b]	4s	−9.17	1.83	–	–	–
	4p	−5.15	1.13	–	–	–
	3d	−13.49	5.75	2.00	0.5683	0.6292

Distinctions in Bonding for $Ta_{11}Si_2Se_8$ and $Ta_{11}Ni_2Se_8$

The isotypic compounds $Ta_{11}Si_2Se_8$ and, e.g., $Ta_{11}Ni_2Se_8$[17d] differ markedly in bonding, although the distances between the interstitial atoms Si and Ni and the nine Ta atoms of the cluster average 262.7 pm in each case. The *c* parameters, however, differ by 7 pm and the *a* and *b* parameter by about 10 pm. The Ta_9Si cluster is stretched along the pseudo-threefold axis and the capping atoms are closer to the centre (274.8 pm) than in the Ta_9Ni cluster (279.6 pm). A similar spectrum of Ta−Si distances for tetrakaidecahedrally coordinated Si is found in binary silicides like Ta_5Si_3 (Mn_5Si_3-type),[23] d_{Si-Ta}: 255.8−281.5 pm. As seen from Figure 8, a shortening of the Ta^c-Ta^{pr} distances in $Ta_{11}Si_2Se_8$ is associated with a shortening of the interprism contacts Ta4−Ta6 by 11.3 pm, and an extension of the intercluster Ta^c-Ta^c contacts by 6.3 pm. The changes in bond length, however, do not perfectly correlate with the changes of the respective MOP values. The distinctive "breathing modes" in the chains −(Ta2−Ta6−Ta1−Ta4−Ta2−Ta3−Ta5−)Ta2 of the two compounds can be traced back to a significant difference between the strength of the $Si-Ta^c$ (<0.27>) and $Ni-Ta^c$ (<0.13>) interactions: Evaluated according to the mean MOP values given in brackets, the bond strengths differ by a factor of two. There are obviously more valence electrons available for heteronuclear bonding in the Ta_9Si than in the Ta_9Ni cluster. Concomitantly, the average Ta−Se and Ta−Ta distances are both 1.1 pm longer for the silicide ($<d_{Ta-Se}>$ = 265.9 pm, $<d_{Ta-Ta}>$ = 316.7 pm) than for $Ta_{11}Ni_2Se_8$.

Substitution of Molybdenum for Tantalum

The major component of $Ta_{11}Si_2Se_8$ can be partly replaced by molybdenum. The partial substitution occurs at the Ta1 position where metal atoms are coordinated similarly to those in *bcc* tantalum itself. This position represents, so to speak, the most reduced centre of the Ta partial structure. It is partly occupied by about 10% molybdenum. The difference between the affinities Mo−Se and Ta−Se, which − according to our observations − is lower in the case of Mo−Se, may serve as a rationale for the enrichment of the minority component Mo at this particular position of the intermetallic framework. At this position, metal atoms have only two Se neighbours; the other crystallographically inequivalent Ta atoms are bound to three or four Se atoms, see Table 4.

Conclusion

(i) Air-sensitive $Ta_{11}Si_2Se_8$ is accessible by application of high-temperature synthesis techniques. Fibrous crystals can be grown by a chemical transport reaction.

(ii) The crystal structure is isotypic with those of

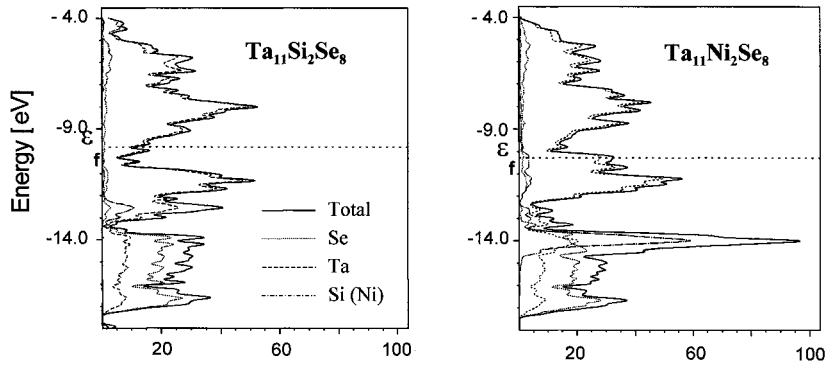

Figure 6. Total DOS and DOS projections of the constituents of (a) $Ta_{11}Si_2Se_8$ and (b) $Ta_{11}Ni_2Se_8$ in the energy window −4 to −18 eV

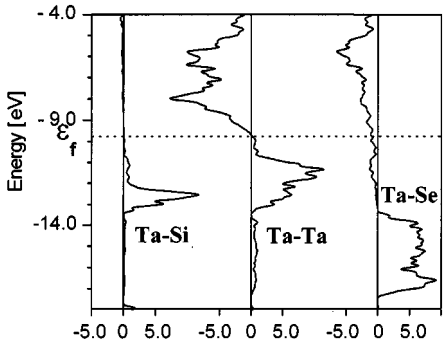

Figure 7. COOP curves of Ta−Ta, Ta−Se, and Ta−Si for $Ta_{11}Si_2Se_8$

$Ta_{11}M_2Se_8$ (M = Fe, Co, Ni). It consists of an open network of condensed tetrakaidecahedral Ta_9Si clusters. The Se atoms have a single-sided Ta coordination; they cover the internal surface of the porous $Ta_{11}Si_2$ partial structure.

(iii) One out of six crystallographically inequivalent Ta atoms, namely Ta1 with the highest valence electron concentration for Ta−Ta bonding, can be partly replaced by molybdenum. The Mo-doped phase is a moderate metallic conductor.

(iv) Semi-empirical band structure calculations reveal striking differences in bonding for the two isotypic phases $Ta_{11}E_2Se_8$ (E = Si, Ni). The heteronuclear bonding interactions between the encapsulated atom and the Ta atoms of the Ta_9E cluster are substantially stronger for the silicide than for the Ni phase. The maximum of the projected DOS of Si is about 1.5 eV above the projected DOS of Ni. As a consequence, only the projected DOS of Si is − at least to a very large extent − energetically separated from the projected DOS of Se through a local minimum in the DOS at about −13.5 eV.

Experimental Section

Synthesis: $Ta_{11}Si_2Se_8$ was prepared in form of a grey, microcrystalline powder from a pre-reacted mixture of the elements in a sealed tantalum tube at 1570 K within 2 d. The pre-reacted mixtures were produced from the elements (Ta: Starck, 99.8%; Si: Heliotronic, 99.99%; Se: Chempur, 99.999%; total: 500−600 mg) in previously outgassed, evacuated quartz glass ampoules at 1170 K within 1 d. Up to 3 mm long and 20 μm thick, silver-shiny, needle-shaped crystals of Mo-doped $Mo_xTa_{11-x}Si_2Se_8$ were produced by a chemical vapour transport reaction in a welded molybdenum crucible starting from a compacted, stoichiometric mixture of $TaSe_2$, Ta, and Si (600 mg) and TeI_4 (8 mg) as a transport agent. The crucible was quickly heated up in an induction furnace, kept at 1870 K for 1 h and cooled down to 1450 K within 8 h. The furnace was then switched off. $TaSe_2$ and TeI_4 were prepared from stoichiometric mixtures of the elements in previously outgassed, evacuated quartz glass ampoules at 1270 K, 3 d ($TaSe_2$) and at 670 K, 3 d (TeI_4, I_2: Merck, 99.99%), respectively.

Phase Analyses: The phases of starting material and product were identified by powder X-ray diffraction measurements employing the Guinier technique (Guinier System 600, Huber; Cu-$K\alpha_1$ radiation). Silicon (a = 543.09 pm) was used as an internal standard. Powder diffractograms (PW1050/25, Philips; Ni-filtered Cu-K_α radiation) were recorded in the range 5° < 2θ < 95°; scan width: 0.03°; scan time per step: 90 s. Rietveld refinements were performed with the program LHPM.[24] The atomic positions as determined by the crystal structure refinement were used as starting parameters. Selected samples were analysed by energy-dispersive X-ray spectrometry (EDX, CS 4DV, CamScan; detector: Noran Instruments). The composition of the Mo-doped crystals was determined to be $Mo_{0.35(9)}Ta_{11.3(5)}Si_{1.2(5)}Se_{8.0(1)}$ by merging five independent analyses. A similar low Si content was also found for the ternary

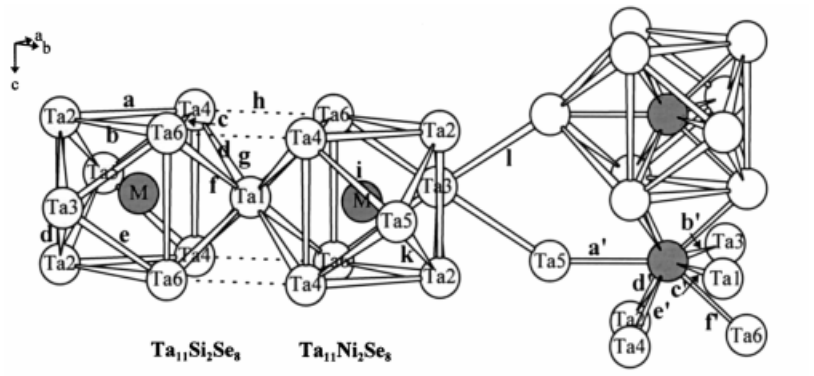

	$Ta_{11}Si_2Se_8$	$Ta_{11}Ni_2Se_8$
a	331.6(0.16)	329.3(0.19)
b	324.5(0.18)	322.3(0.22)
c	316.9(0.21)	320.4(0.20)
d	291.9(0.36)	296.7(0.34)
e	307.5(0.22)	306.7(0.24)
f	288.5(0.32)	291.8(0.33)
g	290.1(0.31)	291.2(0.34)
h	338.1(0.07)	349.4(0.04)
i	305.4(0.27)	304.1(0.30)
k	308.4(0.24)	306.3(0.27)
l	318.4(0.17)	312.1(0.19)

	$Ta_{11}Si_2Se_8$	$Ta_{11}Ni_2Se_8$
a'	277.4(0.29)	281.9(0.13)
b'	275.0(0.28)	282.0(0.13)
c'	272.0(0.25)	275.0(0.12)
d'	253.0(0.37)	248.8(0.26)
e'	256.4(0.35)	255.3(0.24)
f'	256.3(0.35)	252.7(0.25)

Figure 8. Distinct structural features of $Ta_{11}Si_2Se_8$ and $Ta_{11}Ni_2Se_8$ reflected by selected distances and MOP values

phase probably due to the superposition of the Ta-*M* and the Si-*K* emission line.

Electrical Resistivity Measurements: Four-probe dc electrical resistivities of two needle-shaped crystals ($5 \times 10 \times 1000$ μm and $10 \times 20 \times 750$ μm) were measured as a function of temperature in the range 10−325 K. The four copper leads were attached along the needle axis with silver epoxy glue. Details concerning the measurements and the equipment are given elsewhere.[13c]

Crystal Structure Determination: Weissenberg and Buerger precession photographs of a crystal mounted along the needle axis yielded an orthorhombic unit cell. The lattice parameters, intensity modulations and the extinctions pointed unambigously to a phase that is isotypic with $Ta_{11}Ni_2Se_8$, space group symmetry *Pnnm*. Intensity data of two crystals ($0.02 \times 0.02 \times 0.31$ mm and $0.01 \times 0.01 \times 0.16$ mm) were collected employing an imaging plate diffraction system IPDS (Stoe) using Mo-K_α radiation and a graphite monochromator. Direct methods (SHELXS-96[25]) led to the anticipated structure. Application of a semi-empirical absorption correction based on symmetrically equivalent reflections (XPREP, SHELXTL[25]) improved the residual value R_{int} from 0.1047 to 0.0761 for the intensities in the case of the larger crystal. The calculations of the two data sets converged at $wR2 = 0.0631$ and 0.0691. The isotropic displacement parameter of one metal position, namely Ta1 situated in the centre of a Ta_9 cuboid was strikingly large. Nonrestricted refinements of the displacement parameter and a mixed occupation by Ta and Mo yielded in qualitative agreement with EDX analyses 89% (86%) Ta and 11% (14%) Mo and unobstrusive *U* values. Further information concerning the structure determination of the larger crystal is given in Table 2. Structural parameters are listed in Tables 3 and 4.

Acknowledgments

This research was generously supported by the Deutsche Forschungsgemeinschaft, the Fonds der Chemischen Industrie and by H. C. Starck. We thank Dr. Holger Kleinke for aid with the use of the extended Hückel program.

[1] [1a] H. F. Franzen, J. G. Smeggil, *Acta Crystallogr.* **1969**, *B25*, 1736−1741. – [1b] H. F. Franzen, J. G. Smeggil, *Acta Crystallogr.* **1970**, *B26*, 125−129.
[2] B. Harbrecht, *J. Less-Common. Met.* **1988**, *138*, 225−234.
[3] [3a] H. Wada, M. Onoda, *Mater. Res. Bull.* **1989**, *24*, 191−196. – [3b] S. J. Kim, K. S. Nanjundaswamy, T. Hughbanks, *Inorg. Chem.* **1991**, *30*, 159−164.
[4] B. Harbrecht, H. F. Franzen, *Z. Anorg. Allg. Chem.* **1987**, *551*, 74−84.
[5] B. Harbrecht, V. Wagner, C. Pietzonka, *J. Solid State Chem.* **1998**, *139*, 45−51.
[6] [6a] . Harbrecht, V. Wagner, *Z. Anorg. Allg. Chem.* **1994**, *620*, 969−976. – [6b] V. Wagner, Dissertation, University of Dortmund, **1994**.
[7] [7a] M. Conrad, B. Harbrecht, *IVth Eur. Conf. Solid State Chem.*, Dresden **1992**, p. 324. – [7b] M. Conrad, Dissertation, University of Dortmund, **1997**.
[8] T. Degen, B. Harbrecht, *Acta Crystallogr.* **1995**, *C51*, 2218−2220.
[9] M. Conrad, B. Harbrecht, *Z. Anorg. Allg. Chem.* **1997**, *623*, 742−748.
[10] B. Harbrecht, S. Debus, in preparation.
[11] T. Degen, B. Harbrecht, *Angew. Chem.* **1995**, *107*, 2888−2890; *Angew. Chem. Int.Ed. Engl.* **1995**, *34*, 2703−2705.
[12] [12a] M. Conrad, F. Krumeich, B. Harbrecht, *Angew. Chem.* **1998**, *110*, 1554−1557; *Angew. Chem. Int. Ed.* **1998**, *37*, 1383−1386. – [12b] M. Conrad, B. Harbrecht, *Aperiodic '97* (Eds.: M. de Boissieu, R. Currat, J.-L. Verger-Gaugry), World Scientific, Singapore, in press. – [12c] F. Krumeich, M. Conrad, H.-U. Nissen, B. Harbrecht, *Phil. Mag. Lett.* **1998**, *78*, 357−367.
[13] [13a] B. Harbrecht, *Angew. Chem.* **1989**, *101*, 1696−1698; *Angew. Chem. Int. Ed.Engl.* **1989**, *28*, 1660−1662. – [13b] K. S. Nanjundaswamy, T. Hughbanks, *J. Solid State Chem.* **1992**, *98*, 278−290. – [13c] B. Harbrecht, T. Degen, M. Conrad, *J. Alloys Comp.* **1997**, *246*, 37−50. – [13d] X. Yao, G. J. Miller, H. F. Franzen, *J. Alloys Comp.* **1992**, *183*, 7−17. – [13e] X. Yao, H. F. Franzen, *J. Am. Chem. Soc.* **1991**, 1426−1427.
[14] [14a] X. Yao, H. F. Franzen, *J. Alloys Comp.* **1992**, *182*, 299−312. – [14b] T. Degen, B. Harbrecht, *Angew. Chem.* **1995**, *107*, 1226−1228; *Angew. Chem. Int. Ed. Engl.* **1995**, *34*, 1089−1091.
[15] [15a] M. E. Badding, F. J. DiSalvo, *Inorg. Chem.* **1990**, *29*, 3952−3954. – [15b] J. Li, R. Hoffmann, M. E. Badding, F. J. DiSalvo, *Inorg. Chem.* **1990**, *29*, 3943−3952. – [15c] K. Ahn, T. Hughbanks, D. D. Rathnayaka, D. G. Naugle, *Chem. Mater.* **1994**, *6*, 418−423. – [15d] M- E. Badding, R. L. Gitzendanner, R. P. Ziebarth, F. J. DiSalvo, *Mater. Res. Bull.* **1994**, *29*, 327−336. – [15e] J. Neuhausen, E. W. Finck, W. Tremel, *Chem. Ber.* **1995**, *128*, 569−573.
[16] J. M. Tarascon, F. J. DiSalvo, C. H. Chen, J. Carroll, M. Walsh, L. Rupp, *J. Solid State Chem.* **1985**, *58*, 290−300.
[17] [17a] B. Harbrecht, H. F. Franzen, *J. Less-Common Met.* **1986**, *113*, 349−360. – [17b] B. Harbrecht, *J. Less-Common Met.* **1986**, *124*, 125−134. – [17c] B. Harbrecht, *J. Less-Common Met.* **1988**, *141*, 59−71. – [17d] M. Conrad, B. Harbrecht, *J. Alloys Comp.* **1993**, *197*, 57−64. – [17e] M. Conrad, B. Harbrecht, *Z. Kristallogr.*, submitted.
[18] [18a] B. Harbrecht, *J. Less-Common Met.* **1986**, *115*, 177−189. – [18b] X. Yao, H. F. Franzen, *J. Less-Common Met.* **1990**, *161*, L37-L40.
[19] [19a] R. L. Abdon, T. Hughbanks, *Chem. Mater.* **1994**, *6*, 424−428. – [19b] R. L. Abdon, T. Hughbanks, *J. Am. Chem. Soc.* **1995**, *117*, 10035−10040. – [19c] C. Wang, T. Hughbanks, *Inorg. Chem.* **1996**, *35*, 6987−6994.
[20] A. Mrotzek, Dissertation, Philipps University of Marburg, **1998**.
[21] [21a] R. Hoffmann, *J. Chem. Phys.* **1963**, *39*, 1397−1398. – [21b] M.-H. Whangbo, R. J. Hoffmann, *J. Am. Chem. Soc.* **1978**, *100*, 6093−6098.
[22] [22a] T. Hughbanks, R. Hoffmann, *J. Am. Chem. Soc.* **1983**, *105*, 1150−1162. – [22b] M. J. Calhorda, R. Hoffmann, *Inorg. Chem.* **1988**, *27*, 4679−4686.
[23] H. Nowotny, H. Schachner, R. Kieffer, F. Benesovsky, *Monatsh. Chem.* **1953**, *84*, 1−12.
[24] D. B. Wiles, R. A. Young, *J. Appl. Crystallogr.* **1981**, *14*, 149−151.
[25] [25a] G. M. Sheldrick, *SHELXS-96*, University of Göttingen, **1996**. – [25b] G. Sheldrick, *SHELXTL*, *SHELXTL-Plus*, Release 5.0 for R3 Crystallographic Research Systems, Siemens Analytical X-Ray Instruments Inc., Madison, WI, USA, **1991**. – [25c] G. M. Sheldrick, *SHELXL-96*, University of Göttingen,-Germany, **1996**.

Received July 20, 1998
[I98240]